ISBN: 978-3-95450-222-6 ISSN: 2673-5350 doi:10.18429/JACoW-IBIC2020-THPP34

CALIBRATION AND IMAGE RESTORATION FOR THE BEAM PROFILE MEASUREMENT SYSTEM*

L. X. Hu[1], Y. T. Song†, K. Z. Ding,
Institute of Plasma Physics, Chinese Academy of Sciences, Hefei, China
Y. C. Wu, Hefei CAS Ion Medical and Technical Devices Co., Ltd, Hefei, China
[1]also at University of Science and Technology of China, Hefei, China

Abstract

The transverse beam profile parameters are closely related to the beam tuning and optimization of the cyclotron. In order to improve the precision and efficiency of beam profile measurement system, A calibration method has been implemented for the calibration of the imaging system. Moreover, a new image noise reduction algorithm has been developed to improve the image quality, and then to improve the measurement accuracy of the beam profile parameters. In addition, two image restoration algorithms have also been adopted to eliminate the effects of defocusing blur. The experiment results show that the calibration of the imaging system enable the system to provide quantitative information for beam diagnosis. The image noise reduction and restoration algorithm greatly improve the measurement accuracy of beam profile parameters.

INTRODUCTION

The beam profile parameters are one of the important parameters, which represent the beam quality [1]. The performance of the accelerator and the safe and stable operation are closely related to the transverse beam distribution [2]. The measurement of beam profile parameters can provide an important basis for the debugging and commissioning of the accelerator and the improvement of beam quality [3]. The most commonly used beam profile measurement instruments include: Scintillator detector [4], OTR target [5], synchronized light imaging [6] and wire scanning [7].

Due to the limitation of the imaging system and the influence of the imaging and signal transmission environment, there will inevitably be distortion and deviation between the observed image and the actual image, which is called image degradation [8]. The main factors leading to the image degradation of the scintillator detector include：

- The image distortion caused by the aberration and nonlinear distortion of the imaging system;
- Various noises introduced by the imaging system and image transmission process;
- Defocus blur caused by inaccurate focus of the camera.

The phenomenon of image degradation has a significant impact on the image measurement and analysis.

* Work supported by grants 1604b0602005 and 1503062029.
† email address: hulx@ipp.ac.cn

IMAGING SYSTEM CALIBRATION

Basis of Coordinate Transformation

The conversion relationship between the pixel coordinate system and the world coordinate system is given by

$$z_c \cdot \begin{bmatrix} u \\ v \\ 1 \end{bmatrix} = \begin{bmatrix} f_x & 0 & u_0 & 0 \\ 0 & f_y & v_0 & 0 \\ 0 & 0 & 1 & 0 \end{bmatrix} \cdot \begin{bmatrix} \boldsymbol{R}_{3\times3} & \boldsymbol{T}_{3\times1} \\ \boldsymbol{0} & 1 \end{bmatrix} \cdot \begin{bmatrix} x_w \\ y_w \\ z_w \\ 1 \end{bmatrix} = \boldsymbol{M_1 M_2 X_w} \quad (1)$$

where $[u \quad v]$ is the coordinates in the pixel coordinate system, u_0 and v_0 denote the translation amount of the image coordinate system relative to the pixel coordinate system, f is the focal length of the camera, $\boldsymbol{R}_{3\times3}$ represents the rotation matrix, $\boldsymbol{T}_{3\times1}$ represents the translation matrix, $[x_w \quad y_w \quad z_w]$ is the coordinates in the world coordinate system. $\boldsymbol{M_1}$ is called the internal parameter matrix. $\boldsymbol{M_2}$ is called the external parameter matrix.

Camera Distortion

The image distortion of the visual system occurs in the process of imaging. The radial and tangential distortion have great influences on the image. Radial distortion occurs when light rays bend more near the edges of a lens than they do at its optical center. Tangential distortion occurs when the lens and the image plane are not parallel.

The radial distortion is corrected by the Taylor series expansion shown in Eq. (2) and (3):

$$x_c = x(1 + k_1 r^2 + k_2 r^4 + k_3 r^6), \quad (2)$$

$$y_c = y(1 + k_1 r^2 + k_2 r^4 + k_3 r^6), \quad (3)$$

where k_1, k_2 and k_3 are radial distortion coefficients, r represents the distance from the imaging center, (x, y) and (x_c, y_c) are the undistorted and the distorted points.

The tangential distortion is corrected by the following formulas:

$$x_c' = x + [2p_1 y + p_2(r^2 + 2x^2)], \quad (4)$$

$$y_c' = y + [2p_2 x + p_1(r^2 + 2y^2)], \quad (5)$$

where p_1 and p_2 are tangential distortion coefficients of the lens.

Camera Calibration

For stereo applications, these distortions need to be corrected first. To find the internal and external parameters and camera distortion parameters, what we have to do is to provide some sample images of a well-defined pattern (e.g. chess board). Important input data needed for camera

ISBN: 978-3-95450-222-6 ISSN: 2673-5350 doi:10.18429/JACoW-IBIC2020-THPP34

calibration is a set of 3D real world points and its corresponding 2D image points. With these data, some mathematical problem is solved in background to get the distortion coefficients. That is the summary of the whole story. For better results, we need at least 10 test patterns [9].

Through the calibration, the internal parameter matrix of the camera and the distortion coefficients can be calculated. Furthermore, each image can be re-projected to obtain new projection points.

IMAGE DEGRADATION MODEL

Image Noise

Theoretically, noise is generally regarded as unpredictable random errors, which can only be recognized by statistical methods, and can be described by random processes. The digital characteristics of mean, variance, and correlation function are usually used to describe the characteristics of the image noise.

Impulse noise is a common multiplicative noise caused by the external interference to image sensors and transmission channels. Gaussian noise is an additive noise, which is generally generated by photosensitive elements.

Defocus Blur

For the scintillator detector, the ideal imaging formula is shown in Eq. (6):

$$\frac{1}{f} = \frac{1}{u} + \frac{1}{v} \tag{6}$$

where f is the focal length of the camera, u and v are the object distance and image distance, respectively.

However, if the focal length, object distance and image distance in the imaging system do not satisfy the imaging formula, a point on the original image will become a uniformly distributed disk instead of a point.

Therefore, the point spread function (PSF) of the degraded image caused by defocus is shown in Eq. (7):

$$h(x,y) = \begin{cases} \frac{1}{\pi R^2} & x^2 + y^2 \le R^2 \\ 0, & otherwise \end{cases}. \tag{7}$$

where R is the blur radius.

Modelling

For the degradation of the scintillator detector imaging system, the impulse response and noise pollution are considered. Generally speaking, the imaging system is considered as a linear space-invariant system, that is, the degradation result of each pixel in the image only depends on the gray value of the point, rather than the coordinates of the pixel.

Assuming that the original image is $f(x,y)$, the observed image $g(x,y)$ is obtained under the combined action of the PSF $h(x,y)$ and the additive noise $n(x,y)$.The degradation process can be expressed as:

$$g(x,y) = \int_{-\infty}^{+\infty}\int_{-\infty}^{+\infty} f(\alpha,\beta)h(x-\alpha,y-\beta)d\alpha d\beta + n(x,y). \tag{8}$$

Equation (8) can be expressed as:

$$g(x,y) = f(x,y) \otimes h(x,y) + n(x,y). \tag{9}$$

where $\otimes$ represents the spatial convolution. Therefore, it is very important to study the PSF for the establishment and analysis of degradation model.

NOISE REDUCTION

Description of the Algorithm

An impulse noise filter based on image segmentation and region growing (ISRGF) has been proposed for removing high level of impulse noises. The proposed algorithm is composed of two stages. The aim of the first stage is to detect possible image edges according to predefined image edge patterns, and to remove impulse noise temporarily. In the second stage, image edge detection and image edge tacking algorithms have been applied to divide the preliminary denoised image into irregular regions. For each corrupted pixel, an eight-neighbor region-growing algorithm has been designed to generate a computational domain. The weighted mean of the pixels in the computational domain is calculated to replace the current corrupted pixel.

Image Edge Detection

To preserve the edge details of the image, the image edges need to be detected as accurately as possible. However, the image edges are seriously damaged for highly corrupted images. Based on that, a variety of image edge patterns were defined for accurate image edge detection.

Figure 1 shows two typical image edge patterns. The noise-free pixels within the window are divided into two sets by the image edge, which are denoted by $A_{i,j}$ and $B_{i,j}$ respectively. In Fig. 1, the orange filled squares represent pixels at the image edge, the $A_{i,j}$ and $B_{i,j}$ are denoted by blue filled and green filled squares respectively.

The center pixel $p_{i,j}$ is considered to be located on the image edge if Eqs. (10) and (11) are both satisfied:

$$min[min(A_{i,j}) - max(B_{i,j}), min(B_{i,j}) - max(A_{i,j})] \ge th_1, \tag{10}$$

$$max(E_{i,j}) - min(E_{i,j}) \le th_2, \tag{11}$$

where, $max(A_{i,j})$ and $min(A_{i,j})$ represent the maximum and the minimum value in set $A_{i,j}$ respectively, $E_{i,j}$ denotes the set of noise-free pixels at the potential image edge, th_1 and th_2 denote the given thresholds.

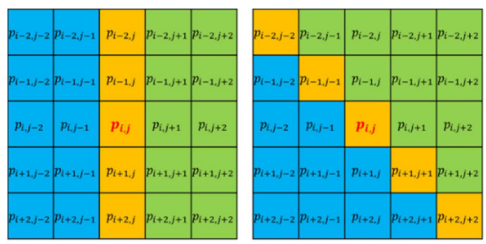

Figure 1: Two typical image edge patterns.

ISBN: 978-3-95450-222-6 ISSN: 2673-5350 doi:10.18429/JACoW-IBIC2020-THPP34

The corrupted pixels are replaced temporarily according to the results of image edge detection. If the corrupted pixel is located on the image edge, it is replaced by the median value of set $E_{i,j}$. Otherwise, it is replaced by the median value of set $A_{i,j}$ or $B_{i,j}$.

Image Segmentation

To achieve the purpose of image segmentation, the Canny edge detector has been adopted to perform edge detection on the preliminary denoised image firstly. Then an edge tracking algorithm has been designed to link the discrete pixels at the adjacent image edge which with similar grey values. Hence, the image edges linked by the edge tracking algorithm are marked with the same number, while discontinuous image edges are marked with different numbers.

The detailed steps of the edge tracking algorithm are described as follows.

1. Scan the image output from the Canny edge detector, and for pixels at image edges, mark the first unmarked pixel (x_0, y_0) with a new number.
2. Check whether the pixel (x, y) in the eight-neighbor of (x_0, y_0) is located on image edges which with similar gray value. If yes, mark it with the same number with (x_0, y_0), and push it into a stack.
3. Extract a pixel from the stack, and take it as (x_0, y_0), then return to step 2).
4. Return to step 1) when the stack is empty.
5. Terminate the procedure until all pixels at image edges are marked.

Figures 2 (a) and (b) show the original image and the result of image edge linking. As can be seen in Fig. 2 (b), the adjacent pixels at image edges which with similar grey values share the same colour, while different image edges are assigned different colours. So that the original image is segmented into many irregular regions by image edges.

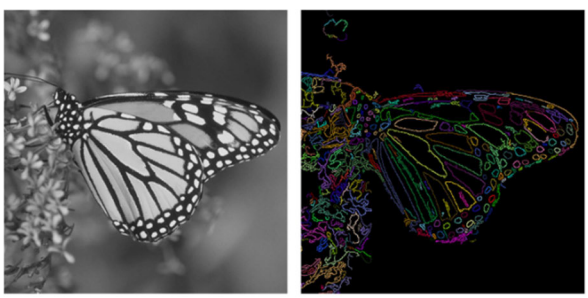

(a) (b)

Figure 2: Image segmentation and image edge linking.

Region Growing

It is obvious that pixels in the same region have similar gray values. Therefore, the corrupted pixel is replaced by the average value of the irregular region which contained the corrupted pixel, instead of the median-type value of the fixed or adaptive windows.

For each corrupted pixel, the eight-neighbour region-growing algorithm has been applied to add adjacent noise-free pixels in the same region into the corresponding computational domain. The computational domain will stop growing when the size of the computational domain or the recursive steps reach the corresponding set value.

Figure 3 shows the results of the region growth in two cases. Different regions are represented by squares filled with different colors. The orange and yellow filled squares denote pixels at image edges. The red filled squares represent the corrupted pixels, and the region surrounded by the red closed dotted line denotes its computational domain.

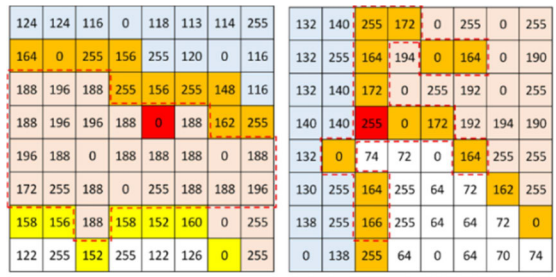

(a) (b)

Figure 3: The results of region growing for (a) corrupted pixel in the texture, (b) corrupted pixel at the image edge.

Weighted Mean Filter

For pixels within the computational domain that are closer to the current corrupted pixel, the higher correlation is considered. Thus, the corrupted pixel is replaced by the weighted mean which defined in Eq. (12).

$$p_{i,j}^{corrupted} = \frac{\sum_{p_{x,y} \in M_{i,j}} w_{x,y} p_{x,y}}{\sum_{p_{x,y} \in M_{i,j}} w_{x,y}} \tag{12}$$

where $M_{i,j}$ is the computational domain of the corrupted pixel $p_{i,j}$, $w_{x,y}$ is the weight of $p_{x,y}$, $d_{x,y}$ is the chessboard distance between $p_{x,y}$ and $p_{i,j}$, and n is a constant.

For isolated corrupted pixel which is surrounded by the image edge, its corresponding computational domain is an empty set. Therefore, the corrupted pixel is replaced by the mean of noise-free pixels in its eight-neighbor.

Quantitative Results Comparison

Several typical images have been tested to assess the quantitative performance of the ISRGF in terms of PSNR (Peak-Signal-to-Noise Ratio) and SSIM (Structural Similarity Index Measure). The grayscale image, namely 'Lena' with size of 512×512 was taken as an example to compare with other representative filters. Different densities of impulse noises varied from 10% to 90% have been added into the test image artificially.

Figure 4 shows the restoration results in terms of PSNR of different filters. It is obvious that the ISRGF has achieved better performance at both low and high noise densities.

ISBN: 978-3-95450-222-6 ISSN: 2673-5350 doi:10.18429/JACoW-IBIC2020-THPP34

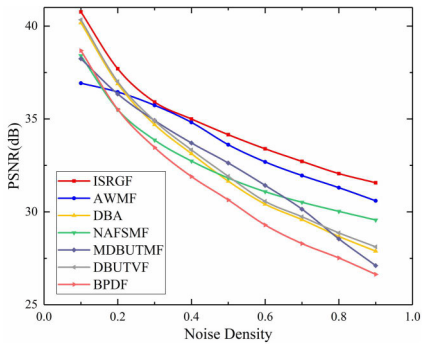

Figure 4: Comparisons of restoration results in PSNR of different algorithms.

IMAGE DEBLURRING

Estimates of the PSF

For the PSF of the defocus blur, the model is uniquely characterized by the defocus radius R. Current estimation methods for defocus radius include: Bessel function analytical method [10], error-parameter analysis method [11] and Laplace operator-based estimation method [12]. According to the advantages and disadvantages of these methods, the estimation method based on Laplace operator is selected to estimate the defocus radius.

Without considering the image noise, second-order differentiation was performed on the blurred image firstly:

$$\nabla^2 g(x,y) = f(x,y) \otimes \nabla^2 h(x,y). \quad (13)$$

Then a fast Fourier transform was performed on the differentiated image to get the self-correlation S of the image:

$$S = \nabla^2 g(x,y) \bowtie \nabla^2 g(x,y)$$

$$S = (f(x,y) \bowtie f(x,y)) * (\nabla^2 h(x,y) \bowtie \nabla^2 h(x,y)) \quad (14)$$

where $\bowtie$ denotes two-dimensional correlation, $S_f = f(x,y) \bowtie f(x,y)$ represents the self-correlation of the original image, $S_h = (\nabla^2 h(x,y) \bowtie \nabla^2 h(x,y))$ represents the self-correlation of the differential PSF function.

From the curved surface image of self-correlation S, it can be seen that there is a sharp peak in the image, which is surrounded by an annular groove [13]. The theoretical value of the radius of the annular groove is the defocus radius. Therefore, the defocus radius can be estimated by identifying the radius of the annular groove, and then the PSF of the defocus model can be determined.

Lucy-Richardson algorithm

Lucy-Richardson algorithm [14] is derived from Bayesian statistics. The basic idea of Lucy-Richardson algorithm is to approximate the maximum likelihood estimation of the original image through iterative calculation. The iterative equation is given by

$$f(x,y)^{n+1} = f(x,y)^n \left[\left(\frac{g(x,y)}{h(x,y) \otimes f(x,y)^n}\right) \bowtie h(x,y)\right] \quad (15)$$

where n is the number of iterations.

Wiener Filter

The principle of Wiener filter is to find an optimal restored image to minimize the mean square error with the original image. Wiener filtering can be expressed as:

$$F(u,v) = \left[\frac{1}{H(u,v)} \cdot \frac{|H(u,v)|^2}{|H(u,v)|^2 + \left[\frac{S_{nn}(u,v)}{S_{ff}(u,v)}\right]}\right] G(u,v) \quad (16)$$

where $K = \frac{S_{ff}(u,v)}{S_{nn}(u,v)}$ is the signal-to-noise ratio. Therefore, when the PSF is obtained, the inverse Fourier transform of the above formula can be performed to obtain the restored image under the specified signal-to-noise ratio.

Wiener filter requires a small amount of calculation, and more importantly, it still has a good restoration effect even for highly corrupted images. However, when the signal-to-noise ratio of the image is small, the restoration effect of Wiener filter will deteriorate.

Results and Analysis

The performance of the Wiener and Lucy-Richardson algorithm was compared in Fig. 5. The blur radius of the blurred image is 10 pixels. It can be seen from Fig. 5 that the performance of the Wiener filter is slightly better than the Lucy-Richardson algorithm. However, the restored image of Wiener filter produces more obvious ringing effect.

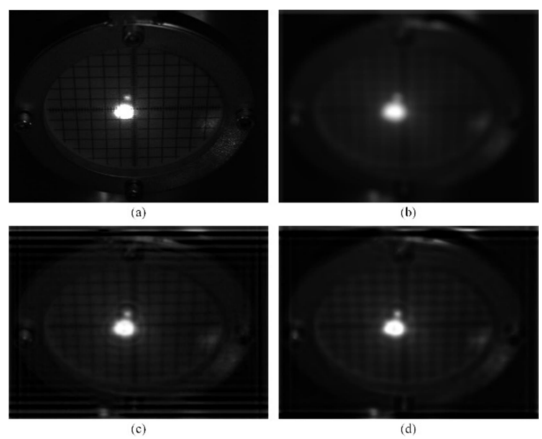

Figure 5: The comparison of the performance of the Wiener filter and Lucy-Richardson algorithm.

CONCLUSION

To improve the precision and efficiency of beam profile measurement system, a calibration method has been conducted for the calibration of the imaging system. Moreover, a new image noise reduction algorithm and two image restoration algorithms have been developed to restore images. The experiment results show that the calibration procedure and image restoration algorithms greatly improve the measurement accuracy of beam profile parameters, which enable the system to provide quantitative information for beam diagnosis.

ISBN: 978-3-95450-222-6 ISSN: 2673-5350 doi:10.18429/JACoW-IBIC2020-THPP34

REFERENCES

[1] J. liu, "Design of the beam profile monitors for compacting THz-FEL source", Master's thesis, University of Science and Technology of China, China, 2016.

[2] B. Walasek-Hohne, C. Andre, P. Forck, *et al.*, "Scintillating screen applications in accelerator beam diagnostics", *IEEE T. Nucl. Sci.*, vol. 59, no. 5, p. 2307-2312, 2012. doi: 10.1109/TNS.2012.2200696

[3] P. Zheng, B. Sun, and P. Lu, "Imaging acquirement system applied to beam profile and emittance measurement for HLS", *Measurement & Control Technology*, vol. 24, no. 5, p. 24-26, 2005. doi: 10.3969/j.issn.1000-8829.2005.05.007

[4] [4] Y. B. Leng et al., "Beam based calibration of X-ray pinhole camera in SSRF", *Chinese Phys. C*, vol. 36, pp. 80-83, 2011. doi:10.1088/1674-1137/36/1/014

[5] P. Forck, "Lecture notes on beam instrumentation and diagnostics", in *Proc. Joint University Accelerator School (JUAS)*, Archamps, France, Mar. 2011.

[6] L. Tang, "Development and Study of Beam Profile Measurement System for HLS II", Ph.D. thesis, University of Science and Technology of China, China, 2012.

[7] M. R. Hadmack and E. B. Szarmes, "Scanning Wire Beam Position Monitor for Alignment of a High Brightness Inverse-Compton X-ray Source", in *Proc. IBIC'13*, Oxford, UK, Sep. 2013, paper WEPF21, pp. 856-859.

[8] H. C. Andrews and B. R. Hunt, "Digital Image Restoration", Englewood Cliffs, New Jersey, USA: Prentice-Hall, 1977. doi:10.1016/0031-3203(79)90032-3

[9] Z. Zhang, "A flexible new technique for camera calibration", *IEEE T. Pattern Anal.*, vol. 22, no. 11, p. 1330-1334, 2000. doi:10.1109/34.888718

[10] S. Treitel, "The complex Wiener filter", *Geophysics*, vol. 39, no. 2, p. 169-173, 1974. doi:10.1190/1.1440419

[11] R. L., Lagendijk, A. M. Tekalp, and J. Biemond, "Maximum likelihood image and blur identification: a unifying approach", *Opt. Eng.*, vol. 29, no. 5, p. 422-436, 1990. doi:10.1117/12.55611

[12] Q. R. Chen, Q. S. Lu, L. Z. Cheng, *et al.*, "Identification of the point spread function from the defocus image using the Laplacian operators", *Computer Engineering & Science*, vol. 27, no. 9, p. 40-43, 2005.

[13] S. Jutamulia, "Joint transform correlators and their applications", in *Proc. SPIE 1812, Optical Computing and Neural Networks*, 1992. doi:10.1117/12.131218

[14] W. H. Richardson, "Bayesian-based iterative method of image restoration", *JoSA*, vol. 62, no. 1, p. 55-59, 1972. doi:10.1364/JOSA.62.000055